Conical crystal spectrograph for high brightness x-ray $K\alpha$ spectroscopy in subpicosecond laser–solid interaction

E. Martinolli, M. Koenig,[a] J. M. Boudenne, and E. Perelli
Laboratoire pour l'Utilisation des Lasers Intenses, UMR7605, CNRS–CEA–Université Paris VI-Ecole Polytechnique, 91128 Palaiseau, France

D. Batani
Dipartimento di Fisica G. Occhialini, Università di Milano-Bicocca and INFM, Via Emanueli 15, 20126 Milan, Italy

T. A. Hall
University of Essex, Colchester CO4 3SQ, United Kingdom

(Received 24 September 2002; accepted 8 March 2004; published online 24 May 2004)

A high brightness crystal spectrograph was designed and successfully used to study the x-ray $K\alpha$ spectrum of aluminum as a diagnostic for target heating due to suprathermal electrons in subpicosecond laser–solid interaction experiments. Conical geometry was chosen in order to enhance spatial focusing, since an extremely low signal-to-noise ratio was expected for the photon flux, and to have a reasonable spectral range while occupying only a small solid angle within the target chamber. Very high image brightness is obtained through strong spatial focusing, as well as good spectral resolution. A simple analytical model and three-dimensional numerical simulation are presented to describe the crystal characteristics. The performance of the spectrograph was tested both on an optical bench and with a ray-tracing code. The experimental spectra allowed us to estimate the target temperature and characterize the fast electron transport. The spectrograph is considered to be particularly useful, in the configuration described here, for high power laser experiments where the solid angle accessible to the spectrograph is small and blast and debris damage from the laser produced plasma is significant. © *2004 American Institute of Physics.*
[DOI: 10.1063/1.1753098]

I. INTRODUCTION

A conically bent crystal spectrograph has been designed and implemented in recent experiments in order to measure the aluminum $K\alpha$ line emission produced by suprathermal electrons. Within the context of inertial confinement fusion, a new approach has been proposed as an alternative to the classical scheme. In this new scheme, the *fast ignitor*,[1–3] nuclear fuel is heated to ignition by relativistic suprathermal electrons[4–7] generated by a subpicosecond laser pulse. The key issue is therefore the amount of energy which can be carried and deposited through the target by the electrons. A few experiments have been performed in order to study energy transport and heating by fast electrons in solid targets. This can be done by means of both optical[8–10] and x-ray diagnostics.[11–14] However, only the latter can give a direct insight into heating in the target bulk.

In our experiment, $K\alpha$ line spectroscopy has been successfully used to determine the stage of ionization of an aluminum fluorescent layer, from which the temperature can then be inferred. As the emitting atoms are ionized by collision with fast electrons, the $K\alpha$ line is shifted towards shorter wavelengths by several tens of mÅ due to lower screening of the nucleus by bound electrons.[15] The ionization stage and associated temperature, which are an important for validating numerical simulations of electron transport, can be estimated from the relative intensities of the shifted lines using nonequilibrium codes. Since the integrated reflectivity of the crystal was absolutely calibrated using an x-ray source (a tantalum cathode), the absolute $K\alpha$ yield could be measured, leading to an estimate of the total energy of incident electrons.

Since the intensity of the these lines is usually weak for the expected range of temperature (~10–50 eV) and the bremsstrahlung noise level can be high, the design of an appropriate spectrograph requires good brightness (photon collection efficiency) and good spectral resolution over the entire *K*-shell spectral range (~7–8.5 Å). Contrary to traditional flat crystals, the conically bent crystal provides strong photon focalization over a long spectral range.[16–18] Moreover, for small Bragg angles, it disperses the spectrum over a shorter and therefore brighter focus line than the Von Hamos crystal[19] and can be bent as easily as a conventional Von Hamos crystal. A property of the conical crystal spectrograph that makes it attractive in laser produced plasma experiments is that the plane to be detected is perpendicular to the axis of the spectrograph. This is particularly important when the detection system is large, such as a streak camera (not in fact used in these experiments). In the design described here, this attribute is used to good advantage by using the crystal at small Bragg angles thereby reducing the solid angle subtended by the instrument at the target. In addition, the design

[a]Electronic mail: michel.koenig@polytechnique.fr

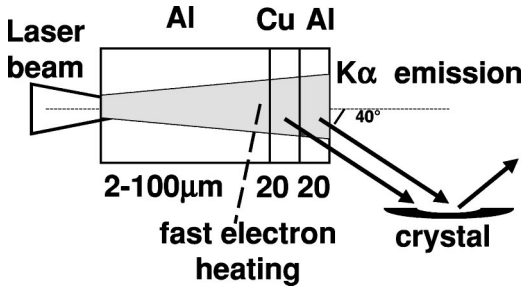

FIG. 1. Experimental setup. The suprathermal electron produced by the laser travels through the target and heats the fluoresced layers, which emit $K\alpha$ radiation collected by the spectrograph.

allows the crystal to be situated a reasonable distance from the target making it easier to protect it from blast and debris damage from the target during a laser shot.

II. EXPERIMENTAL SETUP

A short pulse laser (100 TW at the Laboratoire pour l'Utilisation des Lasers Intenses, Palaiseau, France, and Vulcan at the Rutherford Appleton Laboratory, Chilton, UK) is focused by an off axis parabolic mirror onto a multilayer target, shown in Fig. 1. The small focal spot ($\approx 10\ \mu$m) produces high irradiance (a few $10^{19}\,\mathrm{W\,cm^{-2}}$) on the target. About 10%–30% of the laser energy is transferred to electrons,[4,12] which are accelerated to several 100 keV. The spectrograph looks at the rear side of the target at an angle of 40° from the laser axis, at a distance ≈30 cm from the target. The target is typically composed of three layers. The front propagation layer is made of aluminum of varying thickness (2–100 μm). We do not detect the x rays coming from this layer. Two fluoresced layers were also buried in the target. The first one is copper ($K\alpha$ line at 1.5 Å, detectable in fifth order). The second is aluminum and it emits the shifted $K\alpha$ lines (at ≈8 Å). The ratio of the copper $K\alpha$ line to the aluminum one allows one to estimate the temperature of the fast electron beam, as shown in previous work.[12] Using an electron transport simulation, we estimated the order of magnitude of the expected $K\alpha$ photon flux from the target ($\sim 10^{9}\,\mathrm{srad^{-1}}$). This can be taken as the lower limit. Assuming typical crystal size and reflectivity, one can see that only $\sim 10^{3}$–10^{4} photons will reach the detector. To collect such a weak signal, very strong focus is required. In addition, the physical constraints of the target chamber are such that the spectrograph can occupy only a relatively small solid angle at the target.

III. SPECTROMETER CONFIGURATION

In Fig. 2 a schematic of the conical spectrograph is shown. As first proposed by Hall,[16] the conical geometry is based on modification of the Van Hamos (VH) spectrograph. In the VH, a cylindrical crystal images a polychromatic point source onto a focus segment, both of which lay on the cylinder axis. If the crystal surface is bent on a cone instead of a cylinder, this brings the focused segment onto a vertical axis (parallel to y in Fig. 2) containing the apex of the cone and perpendicular to the nodal line (a line drawn from the apex on the cone surface in the plane containing the cone

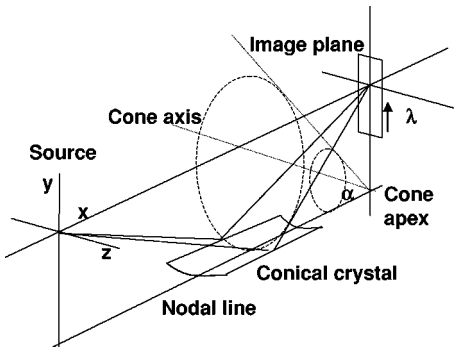

FIG. 2. Schematic of the conical spectrograph. The source is at the origin of the axes. The spectrum focuses on a narrow line in the vertical image plane.

axis and the source). A simple analytical model, based on paraxial ray approximation, can be used to explain this feature, which makes the conical crystal particularly well suited for being coupled to a streak camera for time-resolved spectroscopy. The conical spectrograph can be considered locally an off-axis cylindrical one, in which the radius decreases as it nears the image plane. By using the cylindrical mirror formula,

$$\frac{1}{p}+\frac{1}{q}=\frac{2\sin\theta_c}{r}, \tag{1}$$

referring to Fig. 3, we obtain

$$r(x_c)=-2\frac{y_c}{L}(L-x_c), \tag{2}$$

where $r(x_c)$ is the local radius of curvature of the crystal. We assume an optimum incidence Bragg angle $\theta_c\,(x_c=L/2)$. From Eq. (2) we find that $r=y_c$ and that the cone half angle α is exactly equal to θ_c, as shown in Fig. 3. This implies that for a given angle of incidence there is a best focus condition which determines the position of the source, the position, and the half angle of the cone. This corresponds to the ray falling on the center in Fig. 3. However, this description is oversimplified, because the VH radius r is not exactly local cone radius R. This has two consequences, mainly on the behavior of the oblique rays (striking the crystal at $z\neq 0$): (a) they produce spherical aberrations, which broaden the transversal image size and affect spatial focalization; and (b) rays corresponding to the same wavelength do not focus exactly at the same point (y_i, z_i) on the image plane, thus also affecting the spectral resolution. We will show that these effects can be

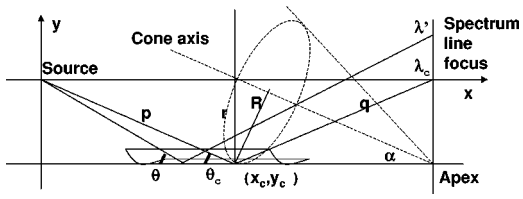

FIG. 3. Schematic diagram (xy plane) of the focalization mechanism of the conical spectrograph. The source is at the origin of the axes, L is the distance between the source and the image plane, (x_c, y_c, z_c) is the point of incidence on the crystal, p and q are incident and reflected rays, and R and r are the local real and approximated crystal radii. Two sets of rays are shown: the center one is the better focused one.

neglected for a given spectral range, provided that the crystal is not too wide. Since an analytical description is quite complicated, we developed a three-dimensional (3D) ray-tracing code to study the spatial and spectral behavior of the spectrograph and choose the actual parameters, taking into account the following constraints. We intended to measure in the spectral range of 7–8.5 Å. Because of the weak photon flux expected, we needed at the same time good integrated reflectivity of the crystal, a large surface, and a close position with respect to the target in order to maximize photon collection. This, in turn, required a small radius, not obtainable for many type of crystals, because of the bad response of the lattice to mechanical strain. As the best choice we adopted a 7×4 cm^2 potassium acid phthalate (KAP) crystal, whose double lattice spacing is $2d=26.64$ Å.[20] The choice of crystal width is discussed below. We fixed the source–crystal distance (310 mm) and best focus ($\lambda=8$ Å), which determines all the other parameters, with respect of the condition seen above. The cone half angle is $\theta=17.48°$ (Bragg angle for 8 Å), the source–detector distance L is 620 mm (limited by the vacuum chamber size), the upper and lower radii of curvature are 93.12 and 78.34 mm, respectively. The 8 mm thick conical surface support of the crystal is made of aluminum and was micromachined with $\pm1\%$ linear precision and $\pm15'$ angular precision (<100 μm). The conical surface was polished to obtain optical quality roughness using different optical metrology techniques. The KAP layer was progressively bent downward to the final radii onto a ''negative'' support block (crystal bending fixture) at very low speed and under controlled temperature and moisture conditions. The crystal is then a fixed to the support. With the help of the 3D ray-tracing code, several features of our spectrograph have been investigated: the focusing power, the dispersion curve, the spectral resolution, and the sensitivity to alignment. In Fig. 4, we show two focus patterns obtained by first dividing the crystal surface into small rectangular cells, in which each node corresponds to the locally reflected ray. This in turn corresponds to a point on the image plane and to a wavelength. The locus of these points with the corresponding wavelength is represented in the surfaces in Fig. 4. The code predicts that reflected rays from the center of the crystal are focused into a narrow peak on the spatial axis (Fig. 4, top). Those coming from the edges fall into two lateral bands outside this peak, causing less efficient photon collection. However, small adjustment in the crystal tilt angle about the z direction allows one to fold the focal surface, thus broadening the peak but collecting the oblique rays better (Fig. 4, bottom). The spectrograph operated close to the second condition. In this case, the predicted spatial size (zi axis) of the focus line is ≈500 μm (≈250 μsm for the brighter center region). The crystal width also affects focusing: since both the image size and solid angle collected increase with the crystal width ($2z_c$), we chose an optimum condition ($z_c/L=0.03$ which gives width $2z_c=4$ cm). As shown in Fig. 5, for $z_c/L<0.03$ the spatial image size $\Delta z_i/L$ remains below 10^{-3}. The spectral image size remains almost constant and $<10^{-4}$ up to $z_c/L\approx0.05$. The average value of dispersion (Fig. 6) is $\Delta x/\Delta\lambda=26.6$ mm/Å, which gives 40 mm for our spectral range. The corresponding Von Hamos would disperse the same range over more than 100 mm. The spectral resolution is given by the following three contributions.

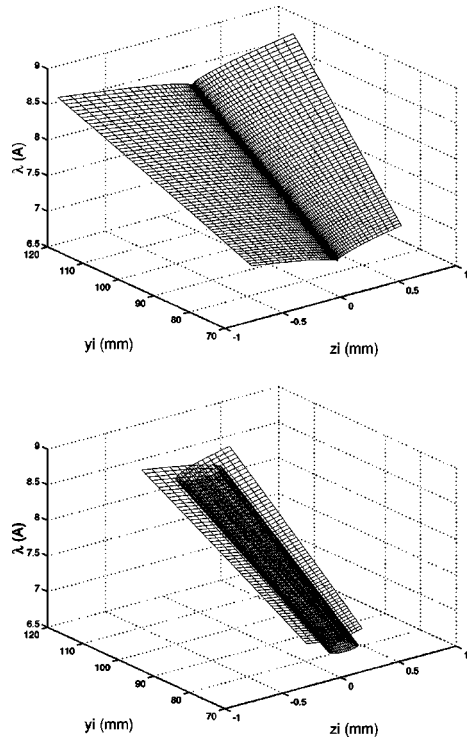

FIG. 4. 3D ray-tracing simulation of the KAP conical crystal: the wavelength is plotted as a function of the focalization grid, at best focus (top) and at the highest ray collection position, in which the focus surface is folded (bottom).

(a) The intrinsic spectral resolution, essentially determined by the imperfection of the lattice $(\lambda/\Delta\lambda)_{\text{int}}$ is in the range of 1000–2000 for a flat KAP crystal. Strong bending like that in our case breaks some atomic bonds, because of stretching/compression of the lattice, especially on the edges, where strong gradients of internal strain are present. This typically degrades the resolution and focalization as much as the radius of curvature is reduced. This point has been checked ex-

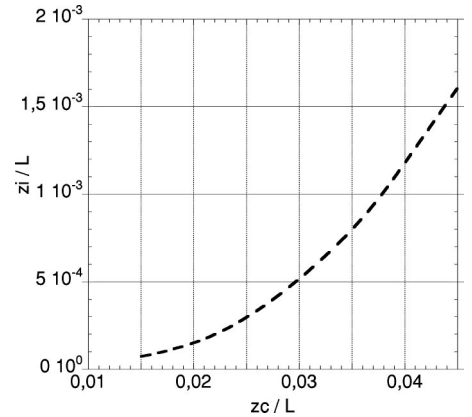

FIG. 5. Spatial image size as a function of the crystal width for a monochromatic source point (8 Å) in best focus (solid line) and in a folded configuration (dashed line). The sizes are normalized over source–detector distance L.

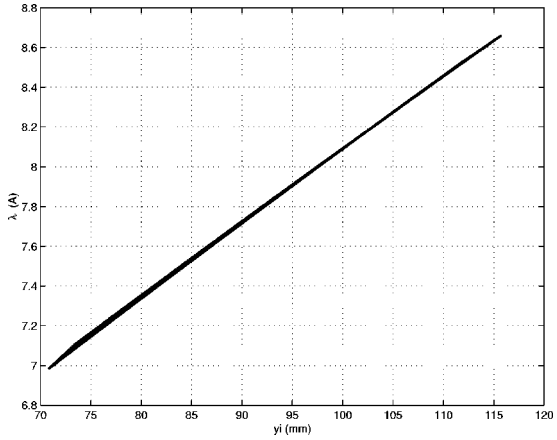

FIG. 6. Dispersion curve obtained with the ray-tracing code.

perimentally (see Sec. IV). A value in the range of 500–1000 seems to be more appropriate.

(b) The spectral resolution due to the detector (Kodak DEF x-ray film read by a 25 μm/px 16 bit densitometer) is $(\lambda/\Delta\lambda)_{\text{det}}>5000$, because of the small pixel size and the good dispersion.

(c) The limiting contribution, one for all spectrally flat crystals, is due to the finite size of the source. In our experiment the emission region can be as large as $\sim$200 μm in diameter. That gives $(\lambda/\Delta\lambda)_{\text{source}}\approx 500$, which corresponds to $\approx$15 mÅ. This is a satisfactory value for our purpose, well below the minimum distance between the two shifted Al $K\alpha$ lines (50–70 mÅ) that we need to resolve.

The image brightness depends on the focusing power of the crystal, i.e., on both the spatial and the spectral image size. For the same source emittance and crystal surface, the ray-tracing code predicts that on the focus line the photon flux is up to 1000 times greater than an equivalent flat crystal. Figure 7 corresponds to a calibration shot on a thin 10 μm aluminum target. In this image, we can clearly see the expected good focusing (Fig. 4). Most of the photons are focused into a narrow line of focus ($\approx$500 μm) but some fall into lateral curved ''wings,'' especially near the brightest spectral lines. As we checked by screening the most oblique rays, defects located mostly at lateral edges of the crystal, produce some irregular lines, superposed on the center focus ($\approx$300 μm).

The image shows Stark-broadened thermal emission lines from the hot laser-side plasma, weakly absorbed in the target. The measured average dispersion is $\Delta x/\Delta\lambda = 26.9$ mm/Å, close to the expected value of 26.6.

The integrated reflectivity was measured with an x-ray

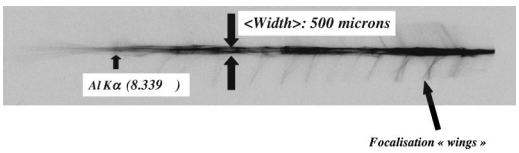

FIG. 7. Focus test shot on an Al 10 μm target. The average width is 500 μm, with a 250 μm center peak.

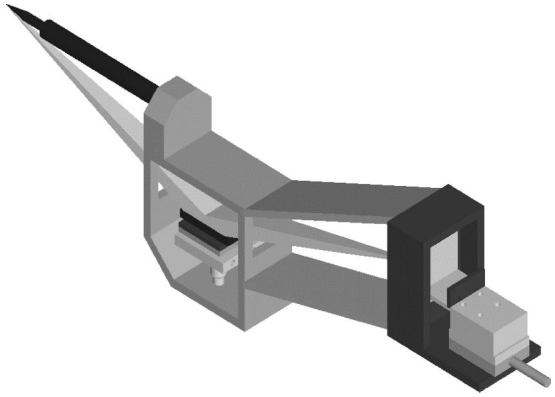

FIG. 8. 3D drawing (without the sidewalls) of the conical crystal spectrograph. On the left, the alignment pin indicates the position of the target. At the center, the crystal is protected from noise by a closed box, which contains also the film holder (shown on the right). Incident and reflected beams are also shown.

calibration source (a tantalum cathode) and was 0.1–0.2 mrad at 1.709 keV (first order) and 0.004–0.01 mrad at 8.146 keV (fifth order).

A two-step alignment procedure has been also designed. (a) First, a 10 μm diam fiber optic was used as a point source on a separate optical bench. The fiber emits visible laser rays which are then reflected by the crystal and focused onto a charge coupled device (CCD) camera. The relative positions and angles are adjusted to obtain the best focus, i.e., the narrowest possible line focus over the whole range of dispersion, as predicted by the ray-tracing code. We used this setup to also validate the results of the code. (b) The spectrograph *as a whole* is then placed into the vacuum chamber and the alignment pin (source point) is brought onto the chamber center by target alignment viewers. A special housing (Fig. 8) was designed to simplify alignment and to provide sufficient screening from x-ray noise and incoming fastparticles. The effect of misalignment of the source was investigated with both the code and the fiber source. Displacement in the *z* direction produces an inverted image in the detector plane but no significant increase in spectral or spatial size. Displacement in *x* is related to the depth of field of the spectrograph and is shown to not increase the image size, whereas a significant increase in image size results from displacing the source on the *y* direction axis a few millimeters. In any case, a finite size source in *x* and *y* produces loss of spectral resolution, as previously discussed. The most crucial adjustment for both the spectral and the spatial resolution seems to be by far the crystal tilt angle about the *z* axis. Rotation of $<1°$ increases the image size by more than a factor of 3–4. These strict positioning requirements and the fact that, *for a given source position relative to the crystal*, the conical crystal works well for *only* one fixed image position are the main constraint of this kind of spectrograph. This is true in the particular geometry we chose which corresponds to what Phillion and Hammel[17] refered to as ''equidistant nontilted.'' This geometry gives the best spectral resolution, but is not the only possible one. Other configurations are possible for the same crystal: for a given source position with respect to the crystal, it will always be possible to find

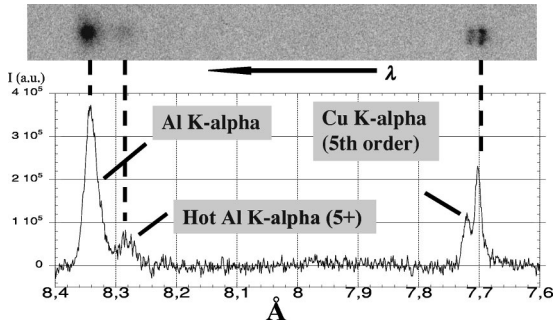

FIG. 9. Experimental spectrum obtained on an Al 11–Cu 25–Al 16 μm target.

a best focus tilt angle of the image plane (for a different Bragg angle and therefore wavelength interval).

IV. EXPERIMENTAL RESULTS

We present in Fig. 9 a spectrum obtained of an Al 11–Cu 25–Al 16 μm target using the conical spectrograph. The cold Al $K\alpha$ line is present as well as the 5+ shifted line. To the right of the image, cold Cu $K\alpha$ I and II lines (reflected at fifth order) are present. With their separation $\approx$19 mÅ, the corresponding spectral resolution $(\lambda/\Delta\lambda)_{\text{expt}}$ is $>$500, as expected. $K\alpha$ lines are produced by fast electrons traveling through the copper and aluminum layers. From these spectra we obtained different kinds of information. The emission spot size can be estimated from the spatial linewidth in the spectrum. The intensity of the $K\alpha$ line versus the thickness gives the fast electron range and temperature, by comparison with an electron transport code.[21] Moreover, the absolute $K\alpha$ yield allows one to infer the total number of incident electrons (and the total energy). The intensity ratio of the cold and hot $K\alpha$ lines allows one to estimate the heat: using an ionization model, we can infer a temperature of 20–30 eV for an $\approx$50 μm target.

ACKNOWLEDGMENTS

The authors gratefully acknowledge G. Robelin (Saint-Gobain Crystals and Detectors, Nemours, France), who was in charge of fabrication of the crystal, J. P. Geindre, P. Audebert, and C. Chenais-Popovics Laboratoire pour l'Utilisation des Lasers Intenses (LULI) for fruitful discussions, as well as support by the LULI and RAL engineering and laser staff. This work was supported by the EU TMR Laser Facility Access Program (Contract No. HPRI-CT-1999-00010) and by the Femto Program of the European Science Foundation.

[1] M. Tabak, J. Hammer, M. E. Glinsky, W. L. Kruer, S. C. Wiks, J. Woodworth, E. M. Campbell, M. D. Perry, and R. J. Mason, Phys. Plasmas **1**, 1626 (1994).
[2] S. Atzeni, Jpn. J. Appl. Phys., Part 1 **34**, 1980 (1995).
[3] Kitagawa *et al.*, Phys. Plasmas **9**, 2202 (2002).
[4] M. H. Key *et al.*, Phys. Plasmas **5**, 1966 (1998).
[5] A. Rousse, P. Audebert, J.-P. Geindre, F. Falliès, J.-C. Gauthier, A. Mysyrowicz, G. Grillon, and A. Antonetti, Phys. Rev. A **42**, 7401 (1994).
[6] F. N. Beg *et al.*, Phys. Plasmas **4**, 447 (1997).
[7] K. B. Wharton *et al.*, Phys. Rev. Lett. **81**, 822 (1998).
[8] E. Martinolli *et al.* (unpublished).
[9] L. Gremillet *et al.*, Phys. Rev. Lett. **83**, 5015 (1999).
[10] J. J. Santos *et al.*, Phys. Rev. Lett. **89**, 025001 (2002).
[11] D. Batani *et al.*, Phys. Rev. E **61**, 5725 (2000).
[12] F. Pisani *et al.*, Phys. Rev. E **62**, R5927 (2000).
[13] M. I. K. Santala *et al.*, Phys. Rev. Lett. **84**, 1459 (2000).
[14] J. A. Koch, M. H. Key, R. R. Freeman, S. P. Hatchett, R. W. Lee, D. Pennington, R. B. Stephens, and M. Tabak, Phys. Rev. E **65**, 016410 (2001).
[15] L. L. House, Astrophys. J., Suppl. Ser. **18**, 21 (1969).
[16] T. Hall, J. Phys. E **17**, 110 (1984).
[17] D. W. Phillion and B. A. Hammel, Rev. Sci. Instrum. **61**, 3738 (1990).
[18] R. Marjoribanks *et al.*, Proc. SPIE **831**, 185 (1987).
[19] L. Von Hamos, Z. Kristallogr. **101**, 17 (1939).
[20] A. Burek, Space Sci. Instrum. **2**, 53 (1976).
[21] L. Gremillet, G. Bonnaud, and F. Amiranoff, Phys. Plasmas **9**, 941 (2002).